# PowerDensityImprovementDueToRotorFluxScreensInAnSrmWithA HigherNumberOfRotorPolesThanStatorPoles

## Ali A. Abdel-Aziz[1], Khaled H. Ahmed[1, 2], Ahmed M. Massoud[3] and Barry W. Williams[1]

[1]Departement of Electronic and Electrical Engineering, University of Strathclyde, Glasgow, G1 1XQ, UK
[2]Department of Electrical Engineering, Alexandria University, Alexandria, 21544, Egypt
[3] Department of Electrical Engineering, Qatar University, Doha, P.O. Box 2713, Qatar

Emails: ali.hassan-abdelaziz-ali@strath.ac.uk, khaled.ahmed@strath.ac.uk, ahmed.massoud@qu.edu.q, barry.williams@strath.ac.uk

## ABSTRACT

This paper studies the performance of screened switched reluctance motors (SRMs) with a number of rotor poles higher than the number of stator poles. Flux (conducting) screens are electrically conducting, non-magnetic materials like aluminum or copper. These screens fill the interpolar rotor air gaps decreasing the unaligned inductance, and thereby increasing the output torque. In addition, flux screens result in a cylindrical rotor structure which minimizes windage losses especially at high speeds. The paper investigates the effect of the flux screens thickness and material on the SRM performance including output torque, power and phase current. A modified flux tube approach for estimating the unaligned inductance of screened SRM is proposed. Finite element analysis results for different screen cases confirm the effectiveness of conducting screens in improving the torque, hence power capability, of switched reluctance motors.

Index-words: Electric vehicles, Finite element analysis, Flux screens, Power density, Renewable energy, Switched reluctance motor, Torque ripple.

## I. INTRODUCTION

In recent years, there has been an increasing interest in replacing conventional fossil fuels for electrical energy generation with renewable energy resources to reduce pollution in an attempt to achieve a green environment. With the transportation sector being a major source of carbon dioxide emissions, researchers are oriented towards electrifying the transportation section [1].

Different electrical machines, including DC, synchronous, and induction machines could be used for propulsion [2], [3]. Conventionally, the rst-choice traction machine is the permanent magnet synchronous machine (PMSM) due to its high torque density, and wide constant torque/ speed range. However, escalated prices and restricted resources of rare-earth materials forced the market to look for a suitable, magnet-free alternative [4].

The switched reluctance machine (SRM) is the dark horse in this race [5]. It has a simple, robust structure, with low cost. Being a double-salient machine with concentrated winding on stator poles, and with neither windings nor permanent magnets on the rotor poles made its design and geometry simpler. Despite the SRM advantages, it suffers from two main drawbacks, namely, vibration and low power density when compared with other traction machines like the PMSM [6] - [8]. Recently, there have been decent attempts to improve the SRM power density [9], [10]. Improving the ef ciency and the power density of the SRM to compete with the PMSM was achieved [11] - [13].

The SRM has been studied extensively in recent decades [14]. A new SRM trend explores a higher number of rotor poles than stator poles, as presented in [15]. The new motor concept ($N_s < N_r$) ($N_s$, $N_r$ are the number of stator and rotor poles, respectively) has lower mass and copper loss than the conventional SRM ($N_s > N_r$). Due to the extra space available in the stator slot area, windings with a higher number of turns and thicker cross-sectional area can be deployed [16]. Also, the rotor pole number increase minimizes torque ripple, which is vital for electric vehicle (EV) applications [17]. However, since the interpolar rotor airgaps are narrower in the new motor design, there is an increase in the unaligned inductance value when compared to that of the conventional SRM. The increase of unaligned inductance reduces the energy conversion area, and hence the produced torque.

In addition, the process of current build-up in the stator winding will be slower due to the decrease in the unaligned inductance value [18]. Hence, to restore the speed of current build-up, a DC link voltage with higher magnitude is required. Also, the salient rotor structure increases the windage loss, especially at high speeds.

Rotor ribs are proposed in [19], [20], to mitigate the SRM windage loss. Film magnetic material is inserted between rotor poles; hence, producing a cylindrical rotor shape. Although the windage loss is signi cantly reduced, the torque density is reduced, and the torque ripple increased, in addition to the mechanical constraints imposed in fabricating the thin magnetic material.

Segmented rotor SRM (SRSRM) with cylindrical rotor design was investigated [21]. However, it suffers from complexity in manufacturing and mechanical weaknesses [22]. In addition, the SRSRM has a longer end winding, which deteriorates the electrical loading of the motor [23]. Also, this motor is not suitable for applications requiring motors with short lamination stack length [24].

The concept of flux screens was proposed in [25]. Interpolar rotor air gaps are filled with materials like copper or aluminium which are electrically conducting materials with non-magnetic properties.  When the rotor rotates with any speed, voltage is induced in the conducting screens, resulting in the flow of eddy currents. A magnetic field is set up by the flow of eddy currents, which opposes the stator main magnetic field. The result is a decrease in the unaligned inductance value. In [25], the impact of utilizing rotor conducting screens on a three-phase 6/4 SRM was investigated. The deployment of rotor conducting screens for three different SRMs was investigated in [26] – [28], where the screened machines produced higher torque levels than unscreened machines with equivalent volume. However, there was no attempt to investigate the SRM performance when varying the thickness or the material of the conducting screen. Also, the low number of rotor poles increases the torque ripple, which is undesirable for EV applications.

In this paper, the utilization of rotor conducting screens for an SRM with a higher number of rotor poles than stator poles ($N_r > N_s$) is investigated. The increased rotor pole number reduces torque ripple. The deployment of rotor conducting screens reduces the unaligned inductance value, hence allowing faster current build-up resulting in higher power per unit volume. Also, as with any SRM, filling the spaces between rotor poles mitigates the windage loss, especially at higher rotor speed. A detailed procedure using the flux tube method for calculating the effective value of unaligned inductance for screened SRMs is presented. Finally, the performance of screened SRM with different screen thicknesses and materials is assessed.

The paper is organized as follows. Section II sheds light on the concept of utilizing rotor conducting screens for SRMs. A method, based on flux tube approach, is discussed in section III to calculate the unaligned inductance value for screened SRM. Supporting 2D and 3D finite element analysis (FEA) results are presented in section IV.

## II.    SRM WITH ROTOR CONDUCTING SCREENS

The SRM structure is simple having salient stator and rotor poles. Only the stator poles have concentrated winding, where each two opposite poles are connected in series forming a phase. In the unaligned position, the flux linkage-current ($\lambda$-$i$) characteristics is linear as the core reluctance is much smaller than the air gap reluctance. On the other hand, when the SRM is in the aligned position core reluctance cannot be ignored resulting non-linear ($\lambda$-$i$) characteristics, as shown in Figure 1.

The conversion area OAB, which is the increase in co-energy when the rotor moves from the unaligned to the aligned position, controls the developed torque. Reducing the effective unaligned inductance increases the conversion area, hence increasing motor output torque. Equation (1) defines the torque.

$$T = \frac{\partial W_f'(\theta, i)}{\partial \theta} \qquad (1)$$

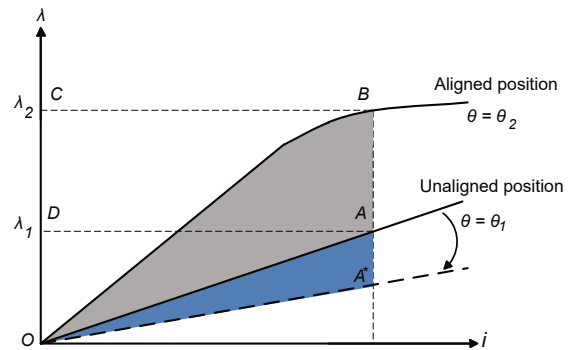where $\theta$ is the rotor position and $W_f'$ is the co-energy



Fig. 1.  Flux linkage-current ($\lambda$-$i$) characteristics of SRM

A new family of SRMs with a higher number of rotor poles than stator poles was presented as in literature. A three-phase 6/10 SRM and a four-phase 8/14 SRM are examples of the new concept. The new SRM can be operated using the traditional asymmetric half-bridge converter [29] and is characterized by reduced torque ripple since $Nr>Ns$, which results in an increased number of strokes per revolution whence increased phase overlap.

Figure 2 shows a three-phase 6/10 SRM. Where, $D_{sh}$, $d$, $D$ are the shaft diameter, rotor diameter, and outer stator diameter, respectively. $h_s$, $h_r$ are the stator and rotor pole heights, respectively. $b_{sy}$, $b_{ry}$ are the stator and rotor back iron, respectively. $\beta_s$, $\beta_r$ are the stator and rotor pole arcs, respectively. $L_g$ is the air gap length, $L$ is the stack length, and $N$ is the number of turns per phase.
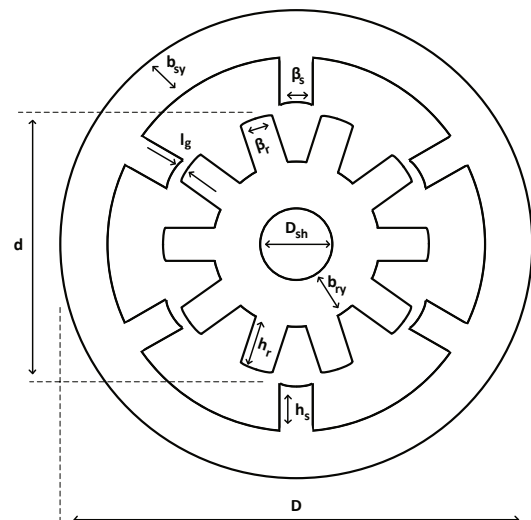


Fig. 2.  Model of 6/10 SRM

For a high number of rotor poles, the available interpolar rotor spaces are narrower when compared with the traditional SRM. Thus, the unaligned inductance is high. Copper or aluminum, which are electrically conducting but non-magnetic materials, are utilized to fill in the interpolar rotor air gaps as shown in Figure 3. Whence, this material is referred to as a conducting screen. When the rotor rotates with any speed, voltage is induced in the conducting screens, resulting in the flow of eddy currents. A magnetic field is set up by the flow of eddy currents, which opposes the stator main magnetic field. The result is a decrease in the unaligned inductance.

## III. FLUX TUBE APPROACH FOR UNALIGNED INDUCTANCE CALCULATION OF SCREENED-SRM

The unaligned inductance effective value is of paramount importance to predict the SRM performance [30]. FEA is an intuitive choice for designing and testing electrical machines. Nevertheless, in the early design stage any change in the SRM geometry, turns number or conduction period, will dictate a new model to be built and simulated. which is a time-consuming process. Hence, starting with a mathematical model is a wise choice which compromises both accuracy and time [31].

This section establishes the unaligned inductance calculation method of screened-SRM using the flux-tube approach [32]. It is worth mentioning that, at the aligned position the screens do not alter the aligned inductance. Five flux paths are used to describe the flux magnetic path at the unaligned position as illustrated in Figure 3.

Figure 4 demonstrates the magnetic equivalent circuit for calculating the screened-SRM unaligned inductance. Where, $R_{sp}, R_g, R_{rp}$, $R_{sy}$ and $R_{ry}$ are the reluctances of the stator pole, air gap, rotor pole, stator back iron, and rotor back iron, respectively.

Flux path reluctances are calculated based on the machine geometrical dimensions. In the unaligned position, core reluctance is insignificant when compared to air gap reluctance. Hence, a linear flux linkage – current ($\lambda$ - i) characteristics curve is obtained.
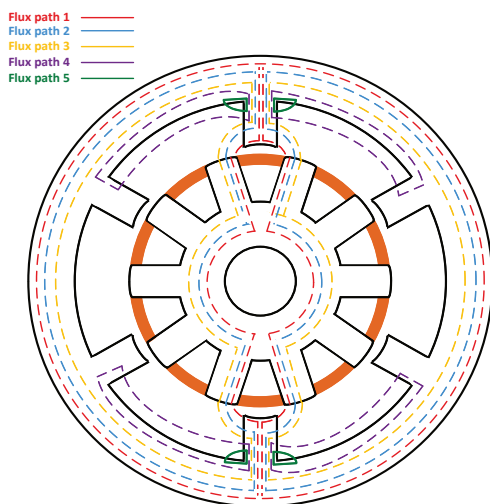


Fig. 3. Flux paths in unaligned position

Generally, reluctance could be expressed by [33], [34].

$$R = l/\mu_0 \mu_r A \qquad (2)$$

where $l$ is the flux magnetic-path length, $A$ is the cross-sectional area, and $\mu_0$ and $\mu_r$ are the permeability of air and core material relative permeability, respectively. The reluctances for the flux paths are derived in detail in the next subsections.
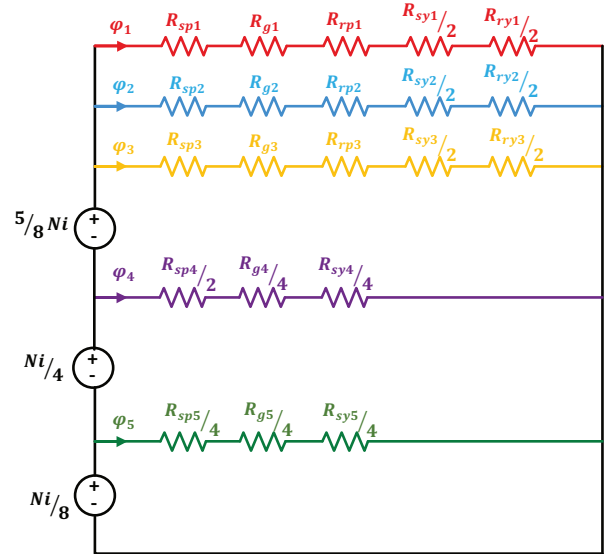


Fig 4. Magnetic equivalent circuit

### A. Flux Paths 1, 2 and 3

The first three flux tubes are similar. Hence, their analysis is combined in this subsection. Figure 5 shows the first magnetic flux path where flux flows through the rotor back iron, the stator back iron, the rotor pole, the stator pole, and finally, the interpolar rotor air gap. Five reluctances are used to describe the magnetic flux path. The magnetic-flux path length and cross-sectional area are calculated as follows:
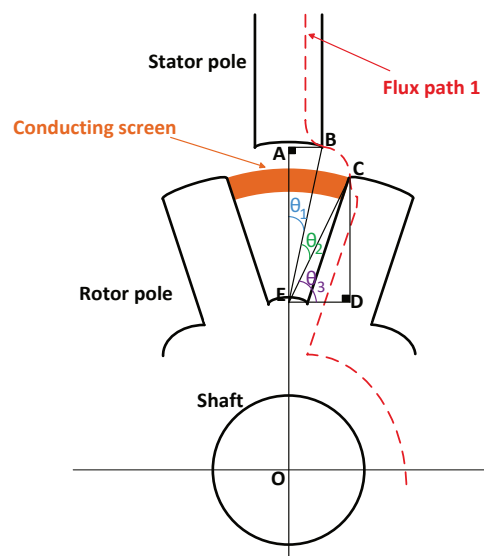


Fig. 5. Flux path 1

## 1. Rotor Back Iron Reluctance, $R_{ry1}, R_{ry2}, R_{ry3}$

For rotor back iron, the average magnetic flux path length and the cross-sectional area are defined by (3) and (4), respectively.

$$l_{ryx} = ½\pi\{D_{sh} + b_{ry}\} \quad (3)$$

$$A_{ryx} = L\,b_{ry} \quad (4)$$

where, $x$ =1, 2, 3 represents flux paths 1, 2 and 3, respectively.

## 2. Stator Back Iron Reluctance, $R_{sy1}, R_{sy2}, R_{sy3}$

Equations (5) and (6) define the average magnetic flux path length and the cross-sectional area for the stator back iron.

$$l_{syx} = ½\pi\{D - b_{sy}\} \quad (5)$$

$$A_{sx} = L\,b_{sy} \quad (6)$$

## 3. Rotor Pole Reluctance, $R_{rp1}, R_{rp2}, R_{rp3}$

For the first three flux paths, the flux travels through the entire rotor pole height. Hence, the average magnetic flux path length is given by (7), where (8) defines the cross-sectional area.

$$l_{rpx} = h_r \quad (7)$$

$$A_{rpx} = \begin{cases} L(½d - l_g)⅜\beta_r^{rad} & ,flux\ path\ 1 \\ L(½d - l_g)½\beta_r^{rad} & ,flux\ path\ 2 \\ L(½d - l_g)⅛\beta_r^{rad} & ,flux\ path\ 3 \end{cases} \quad (8)$$

## 4. Stator Pole Reluctance, $R_{sp1}, R_{sp2}, R_{sp3}$

For path 1, the flux is assumed to leave the stator at the pole tip. For paths 2 and 3, the flux is assumed to leave the stator at 1/10 and ¾ of the stator pole height from the top, respectively. Hence, the length of the flux path is defined by (9).

The width of the flux path determines the area. For flux path 1, the area is assumed to have width ½ $\beta_s$+¼ $h_s$. For paths 2 and 3, the entire flux flows throughout the pole height at a width ½ $h_s$ and ⅛ $h_s$, respectively. The area is then defined by (10).

$$l_{spx} = \begin{cases} h_s & ,flux\ path\ 1 \\ 0.9h_s & ,flux\ path\ 2 \\ ¼h_s & ,flux\ path\ 3 \end{cases} \quad (9)$$

$$A_{spx} = \begin{cases} L(½d\beta_s^{rad} + ¼h_s) & ,flux\ path\ 1 \\ ½Lh_s & ,flux\ path\ 2 \\ ⅛Lh_s & ,flux\ path\ 3 \end{cases} \quad (10)$$

## 5. Air Gap Reluctance, $R_{g1}, R_{g2}, R_{g3}$

The average magnetic flux path length for the air gap is the arc BC as illustrated in Figure 5 and defined by (11)

$$l_{gx} = BC = ½(EB+EC)_2^{rad} \quad (11)$$

When calculating the cross-sectional area involving large air gaps, fringing cannot be neglected. Hence, the area is considered to be the sum of the rotor area defined by (8) and the stator area given by (10).

Finally, the inductance for each flux path is calculated using:

$$L_{ux} = \frac{N^2}{R_{gx} + R_{spx} + R_{rpx} + ½R_{syx} + ½R_{ryx}} \quad (12)$$

### B. Flux Path 4

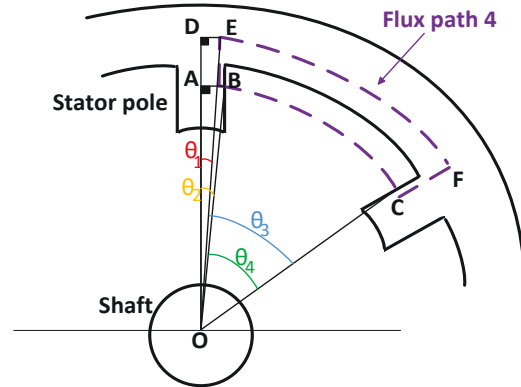Flux path 4 is demonstrated in Figure 6.



Fig. 6. Flux path 4

In this magnetic flux path, the rotor is not involved as the flux lines cross from one stator pole to the adjacent through the air gap and then returns back through the stator back iron. Hence, the three reluctances, $R_{g4}, R_{sp4}$, and $R_{sy4}$, could be calculated as follows:

## 1. Air Gap Reluctance, $R_{g4}$

The arc $BC$ represents the average flux path length in the air gap as given by (13)

$$l_{g4} = BC = (OB)_4^{rad} \quad (13)$$

The cross-sectional area is defined by:

$$A_{g4} = L\frac{h_s}{16} \quad (14)$$

## 2. Stator Pole Reluctance, $R_{sp4}$

The flux is assumed to leave the stator pole at ¾ $h_s$ of the pole height from the top. Therefore, the average magnetic flux path length and the cross-sectional area are defined by (15) and (16), respectively for the stator pole reluctance.

$$l_{sp4} = \frac{1}{4}h_s \qquad (15)$$

$$A_{sp4} = L\frac{h_s}{16} \qquad (16)$$

### 3. Stator Back Iron Reluctance, $R_{sy4}$

The arc EF is the magnetic flux path length for the stator back iron reluctance, which is defined by

$$l_{sy4} = EF = (OE)\theta_3^{\,rad} \qquad (17)$$

On the other hand, the cross-sectional area is expressed by:

$$A_{sy4} = Lb_{sy} \qquad (18)$$

The flux does not link the entire number of turns per phase, $N$. It only links $\frac{3}{8}$ of the turns number. Therefore, the fourth flux path inductance, $L_{u4}$ is given by:

$$L_{u4} = \frac{(\tfrac{3}{8}N)^2}{\tfrac{1}{2}R_{sp4} + \tfrac{1}{4}R_{g4} + \tfrac{1}{4}R_{sy4}} \qquad (19)$$

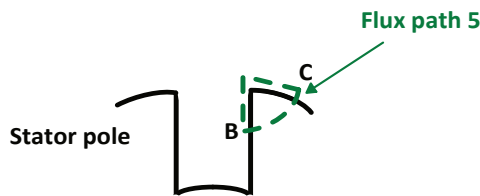### C. Flux Path 5

Figure 7 illustrates flux path 5.



Fig. 7.  Flux path 5

The flux leaves the stator pole to enter the stator back iron, passing through the air gap. The flux path is assumed to represent the perimeter of a quarter circle with center at point $A$ and radius of a quarter the stator pole height $\frac{1}{4}h_s$. The reluctances are calculated as follows:

### 1. Air Gap Reluctance, $R_{g5}$

The arc BC represents the length of the magnetic flux path and defined by (20). While, (21) defines the area.

$$l_{g5} = \frac{1}{2}\pi\frac{h_s}{4} \qquad (20)$$

$$A_{g5} = L\frac{h_s}{16} \qquad (21)$$

### 2. Stator Pole Reluctance, $R_{sp5}$

For the stator pole reluctance, the flux path length is defined by (22), and the area is expressed by (23).

$$l_{sp5} = \frac{1}{4}(h_s + b_{sy}) \qquad (22)$$

$$A_{sp5} = L\frac{h_s}{16} \qquad (23)$$

### 3. Stator Back Iron Reluctance, $R_{sy5}$

The mean flux path length and the cross-sectional area for the stator back iron reluctances are defined by (24) and (25), respectively.

$$l_{sy5} = \frac{1}{4}h_s \qquad (24)$$

$$A_{sy5} = Lb_{sy} \qquad (25)$$

The flux links only $\frac{1}{8}$ the turns per phase $N$. Therefore, , which represents flux path 5 inductance is given by:

$$L_{u5} = \frac{(\tfrac{1}{8}N)^2}{\tfrac{1}{4}R_{sp5} + \tfrac{1}{4}R_{g5} + \tfrac{1}{4}R_{sy5}} \qquad (26)$$

Finally, the effective value of unaligned inductance for the screened- SRM is calculated by summing all the flux path inductances as expressed by (27).

$$L_{ueff} = \sum_{k=1}^{5} L_{uk} \qquad (27)$$

## IV.  SIMULATION RESULTS

In this section, the performance of the screened-SRM is investigated statically and dynamically using FEA. The static test gives an insight on the effective value of unaligned inductance to validate the proposed mathematical approach. On the other hand, the dynamic test studies the effect of varying the thickness and material of the screen on the developed torque and the current build-up process. A three-phase, 6/10 SRM with the specification in Table 1 is used for analysis.

The increased number of rotor poles allows for more space to accommodate the stator winding (since pole arcs of the new SRM are narrower than the pole arcs of a conventional three-phase SRM). According to the selected specification, the copper current density is less than $5A/mm^2$, thus special cooling is not required. For a fair comparison between unscreened and screened SRMs, the same firing angles are applied in both cases.

TABLE I.  SRM SPECIFICATION

| Parameter | Value |
| --- | --- |
| No. of phases $m$ | 3 |
| Stator/rotor poles | 6/10 |
| Number of turns per pole $N$ | 60 |
| Phase winding resistance $R$ | 0.8Ω |
| DC link voltage | 500V |
| Rated power | 6kW |
| Base speed | 1500rpm |

| Axial length | 240mm |
|---|---|
| Shaft diameter | 40mm |
| Rotor outer diameter | 120mm |
| Rotor yoke thickness | 30mm |
| Ratio of rotor pole arc to pole pitch | 0.335 |
| Stator inner diameter | 122mm |
| Stator outer diameter | 200mm |
| Stator yoke thickness | 25mm |
| Ratio of stator pole arc to pole pitch | 0.21 |

### A. Static Analysis

The proposed mathematical approach for unaligned inductance calculation is validated by a 3D FEA model. Table II shows good agreement between the proposed analytical method and the 3D FEA model.

TABLE II.   UNALIGNED INDUCTANCE

| Analytical | 3D FEA |
|---|---|
| 4.66mH | 5.05mH |

The inductance pro le of the SRM under test is plotted in Figure 8 for both the screened and unscreened (original) SRMs.
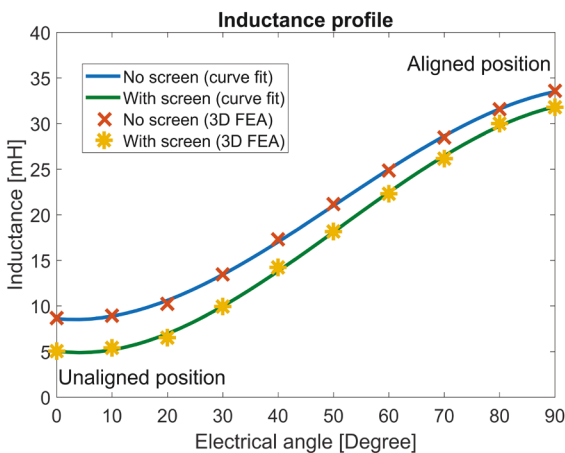


Fig. 8.   Inductance pro le

Results are obtained using 3D FEA model. As expected, the ux screens have insigni cant effect on the aligned inductance value. On the other hand, the unaligned inductance value decreased from 8.68mH in case of unscreened SRM to reach 5.05mH for the screened SRM.

The 40% reduction in the effective unaligned inductance value will increase the conversion area (area OAB in Figure 1) resulting in more developed torque, hence increasing the torque/power density of the SRM.

### B. Dynamics Analysis

The dynamic performance of the screened-SRM is presented in this sub-section using 2D FEA where the process of current build-up along with the developed torque are demonstrated. Conventional asymmetric half-bridge with two diodes and two switches per phase is used. The SRM operates in a single-pulse mode; that is, the dc-link voltage is applied for the whole dwell period. Then a negative voltage is applied at the end of the dwell period for rapid current commutation, as implied in Figure 9.
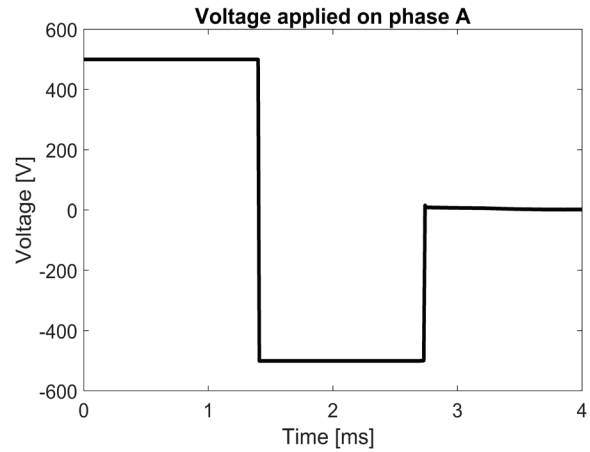


Fig. 9.   The voltage applied on phase A

The dynamic performance at rated conditions is investigated, and Figure 10 compares the results of unscreened and 6mm thick Cu screened SRMs.

Figure 10a shows the phase current waveforms for the unscreened and screened SRMs. The reduction in the effective unaligned inductance alters the current response of the SRM with conducting screens. Utilizing the same dc-link voltage, the screened motor accelerates the current build-up. The rms phase current increases from 17.7A for the unscreened SRM, to 21A for the screened case. Figure 10b compares the torque pro le in both cases. The screened motor is able to develop more torque as a result of a higher current and lower unaligned inductance.

The average torque of the unscreened motor is 38.6Nm. This value increases by 34% to 50.77Nm for the screened SRM, hence improving SRM torque/volume. Thus, the deployment of conducting screens improves the Nm/A by 10%, which re ects on the motor power factor [5].
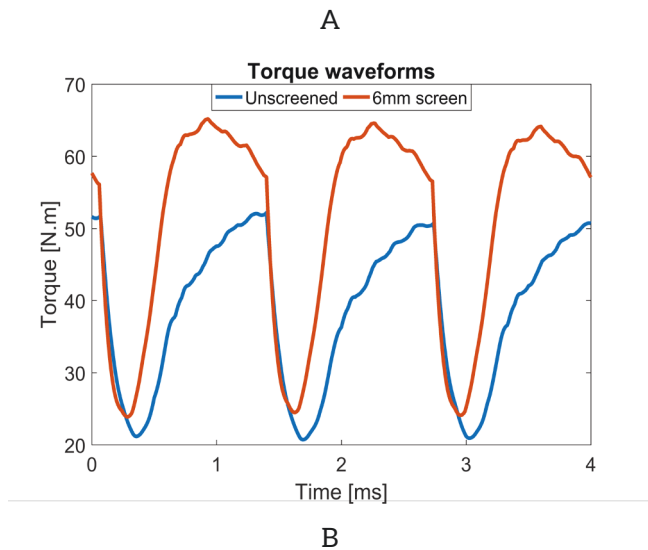
A



B
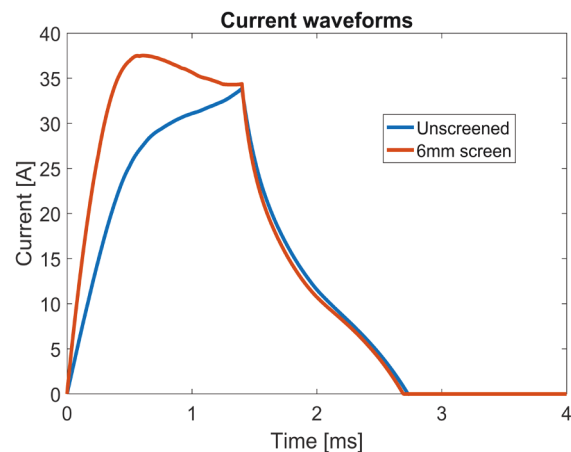
Fig. 10. Performance comparison of unscreened and screened SRM: (a) phase current waveforms and (b) developed torque waveforms.

Figure 11 shows the torque/speed characteristics of the unscreened and screened SRM. The screened SRM offers superior torque over the entire speed range.
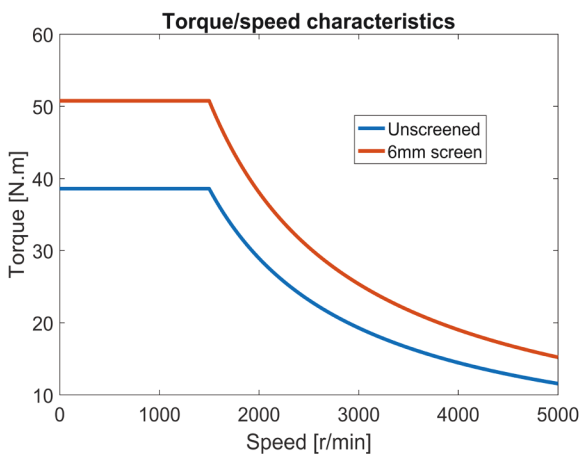


Fig. 11. Torque/speed characteristics

Below the motor base speed, current chopping control (CCC) is used. In this control technique, the motor develops its rated torque, and the speed is controlled from zero up to base speed by controlling the phase currents. Above base speed, the phase currents cannot be controlled (chopped) anymore, and the motor enters the single pulse mode. In this mode, the speed of the motor is controlled by adjusting the turn on and turn off angles. Hence, this mode is referred to as advance angle control (AAC). Above the base speed, the motor cannot produce its rated torque. However, controlling the turn on/off angles allows the motor to operate at constant power.

### C. Effect of Screen Material and Thickness

This subsection investigates the screened-SRM performance when screens with different materials and thicknesses are utilized.

Figure 12 shows SRM current and torque waveforms using two different screens. The rst screen is 3.5mm thick copper, while the second screen is 10 mm thick aluminum (lling the whole interpolar rotor air gaps).
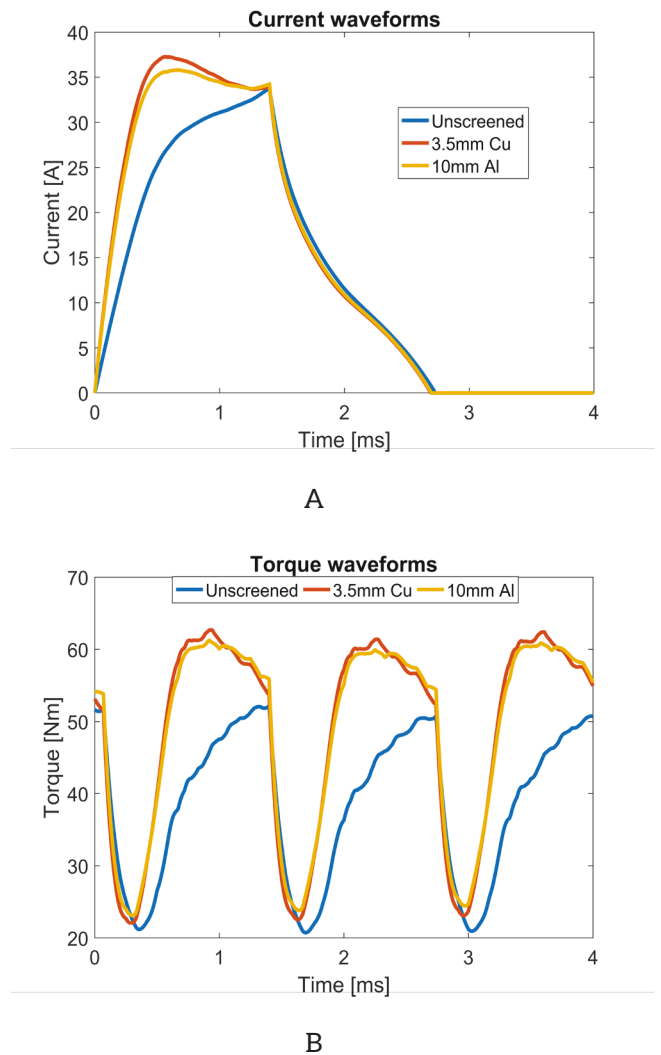


A



B

Fig. 12. Performance of SRM using different screen materials: (a) current waveforms and (b) torque waveforms

The electrical conductivity of copper is $5.98 \times 10^7$ $S/m$ with density 8960 $kg/m^3$. The electrical conductivity of aluminum is $3.5 \times 10^7$ $S/m$ with density 2600 $kg/m^3$. The SRM with a 3.5 mm copper screen is able to deliver the same output torque as the 10 mm aluminum screen. This establishes that electrical conductivity plays an important role in the behavior of the induced eddy current.

Figure 13 compares SRM performance when different thickness copper screens are deployed, where increasing the screen thickness results in more developed torque.

From this study, it is concluded that the thickness and material of the screen affect the SRM performance. Using a lm screen with low conductivity results in higher resistance to the induced voltage, hence the eddy current is smaller. Increased resistivity does result in a reduced eddy current decay time constant.
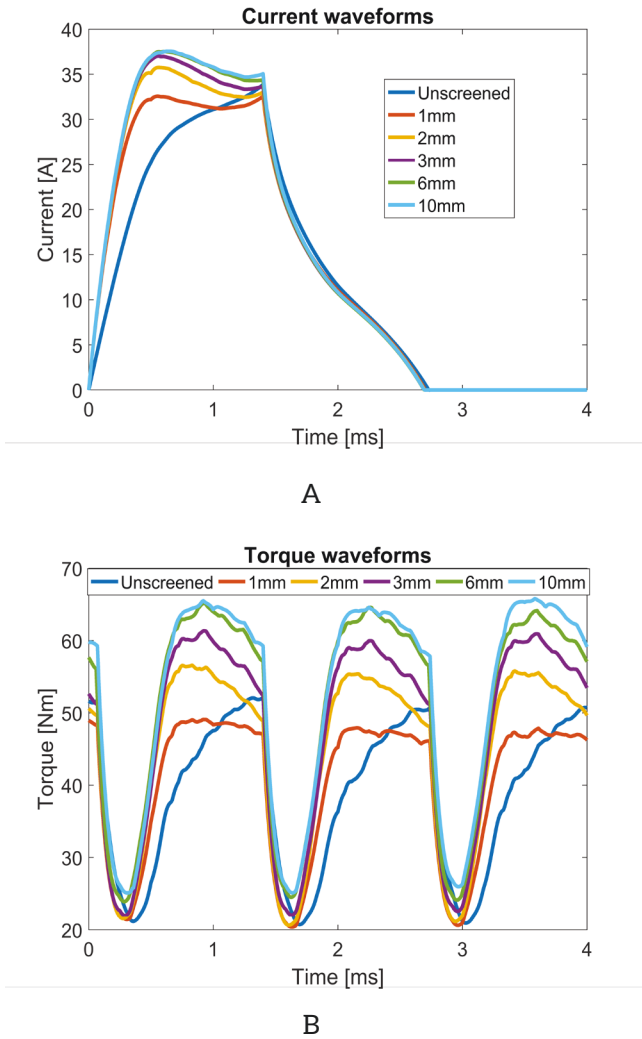
A



A



B

Fig. 13. Performance of SRM using different screen thicknesses: (a) current waveforms and (b) torque waveforms
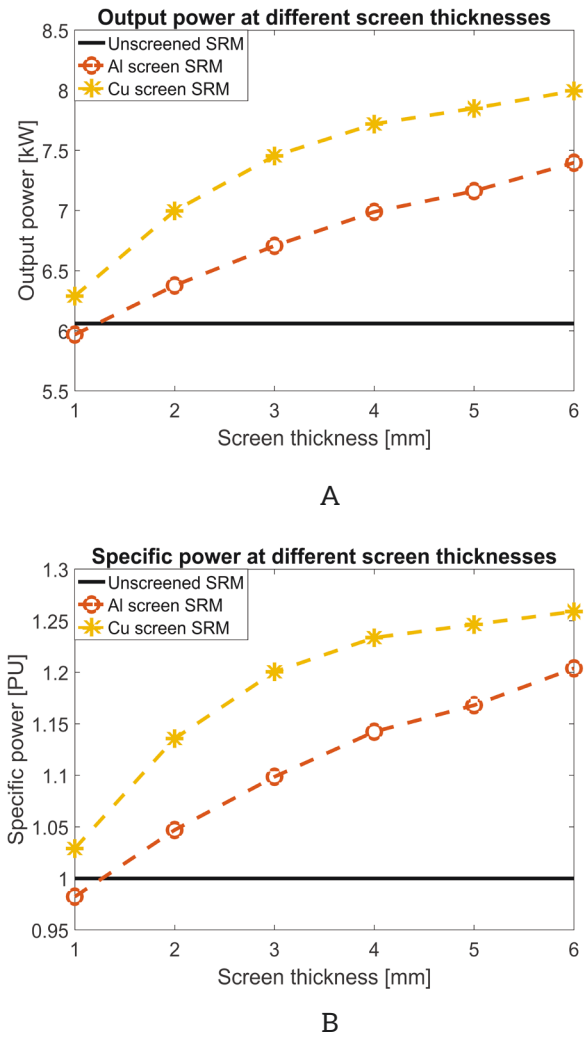


B

Fig. 14. Performance comparison of unscreened and screened SRMs: (a) output power and (b) specific power

The deployment of rotor conducting screens does not alter motor physical volume (as opposed to material volume).

Hence, the increase in output power will directly reflect the increase in power density (kW/litre), as shown in Figure 14a. The specific power (kW/kg) (which is an important factor in most applications) is compared for the unscreened and screened SRMs in Figure 14b, showing an improvement in specific power when conducting screens are used. The penalty for reducing torque ripple and improved torque and power output is screen eddy losses, which reduce machine efficiency.

## VII. CONCLUSION

The paper investigated the effect of utilizing rotor conducting screens to enhance the torque capability of SRM with a higher number of rotor poles than stator poles. The rotor pole increase reduces torque ripple. However, since the interpolar rotor gaps are narrower in the new motor design, the unaligned inductance is significantly higher when compared with conventional SRM, thus reducing the conversion area. Filling the rotor interpolar gaps with electrically conducting, non-magnetic material reduces the effective unaligned inductance as a result of the opposing flux generated by eddy currents in the screens. A detailed derivation of the effective value of unaligned inductance for screened SRM was presented and validated using FEA. A 40% reduction in the unaligned inductance and a 34% increase in output torque was recorded using copper screens. Also, a 10% increase in the Nm/A, hence power factor improvement, was achieved. The effect of using conducting screens of different materials and thicknesses on SRM performance was presented. The SRM with copper screens is able to

deliver more output torque. On the other hand, aluminum is lighter and cheaper. Increasing screen thickness increases torque production. Finally, screened SRMs provided better power density and specic power than unscreened SRM.

Some interesting topics could further be investigated as:

- The performance of SRM with rotor conducting screens has been reported only for motoring mode. The research could be extended to cover the generating mode.

- Given the simple coil winding arrangement in the SRM, and water cooling, advanced manufacturing techniques may offer higher copper density (slot ll factor) improvement possibilities, for example with square section conductors.

## References

[1] Z. Wang, T. W. Ching, S. Huang, H. Wang, and T. Xu, "Challenges Faced by Electric Vehicle Motors and Their Solutions," IEEE Access, vol. 9, 2021, doi: 10.1109/ACCESS.2020.3045716.

[2] E. Sayed et al., "Review of Electric Machines in More-/Hybrid-/Turbo-Electric Aircraft," IEEE Transactions on Transportation Electrication, vol. 7, no. 4. 2021. doi: 10.1109/TTE.2021.3089605.

[3] L. Vadamodala et al., "Comparison of Electric Machine Types for Electrically Driven Engine Accessories Using Multiphysics Simulation Tools," IEEE Trans Ind Appl, vol. 57, no. 2, 2021, doi: 10.1109/TIA.2020.3048095.

[4] E. Bostanci, M. Moallem, A. Parsapour, and B. Fahimi, "Opportunities and Challenges of Switched Reluctance Motor Drives for Electric Propulsion: A Comparative Study," IEEE Transactions on Transportation Electrication, vol. 3, no. 1, 2017, doi: 10.1109/TTE.2017.2649883.

[5] K. M. Rahman, B. Fahimi, G. Suresh, A. V. Rajarathnam, and M. Ehsani, "Advantages of switched reluctance motor applications to EV and HEV: design and control issues," IEEE Trans Ind Appl, vol. 36, no. 1, 2000, doi: 10.1109/28.821805.

[6] A. K. Sahu, A. Emadi, and B. Bilgin, "Noise and Vibration in Switched Reluctance Motors: A Review on Structural Materials, Vibration Dampers, Acoustic Impedance, and Noise Masking Methods," IEEE Access, 2023, doi: 10.1109/access.2023.3257124.

[7] C. A. Wiguna et al., "Vibration and Acoustic Noise Reduction in Switched Reluctance Motor by Selective Radial Force Harmonics Reduction," IEEE Open Journal of Industry Applications, vol. 4, 2022, doi: 10.1109/ojia.2022.3229849.

[8] Y. Yasa, Y. Sozer, and M. Garip, "Acoustic Noise Mitigation of Switched Reluctance Machines With Leaf Springs," IEEE Transactions on Industrial Electronics, vol. 70, no. 2, 2023, doi: 10.1109/TIE.2022.3159969.

[9] A. Sohrabzadeh, H. Torkaman, and A. Y. Javid, "Improvement Undesirable Characteristics of the Switched Reluctance Motor with Triangular Rotor Structure," IEEE Transactions on Energy Conversion, pp. 1–8, 2023, doi: 10.1109/TEC.2023.3265692.

[10] K. Diao, G. Bramerdorfer, X. Sun, Z. Yang, and S. Han, "Multiobjective Design Optimization of a Novel Switched Reluctance Motor With Unequal Alternating Stator Yoke Segments," IEEE Transactions on Transportation Electrication, vol. 9, no. 1, 2023, doi: 10.1109/TTE.2022.3174337.

[11] M. Abdalmagid, M. Bakr, and A. Emadi, "A Linesearch-Based Algorithm for Topology and Generative Optimization of Switched Reluctance Machines," IEEE Transactions on Transportation Electrication, pp. 1–1, 2023, doi: 10.1109/TTE.2023.3245992.

[12] A. Chiba et al., "Torque density and efciency improvements of a switched reluctance motor without rare-earth material for hybrid vehicles," IEEE Trans Ind Appl, vol. 47, no. 3, 2011, doi: 10.1109/TIA.2011.2125770.

[13] K. Kiyota, S. Nakano, and A. Chiba, "A Fast Calculation Method of Optimal Ratio of Outer Diameter and Axial Length for Torque Improvement in Switched Reluctance Motor," IEEE Trans Ind Appl, vol. 54, no. 6, 2018, doi: 10.1109/TIA.2018.2850024.

[14] J. W. Jiang, B. Bilgin, and A. Emadi, "Three-Phase 24/16 Switched Reluctance Machine for a Hybrid Electric Powertrain," IEEE Transactions on Transportation Electrication, vol. 3, no. 1, 2017, doi: 10.1109/TTE.2017.2664778.

[15] P. C. Desai, M. Krishnamurthy, N. Schoeld, and A. Emadi, "Novel switched reluctance machine conguration with higher number of rotor poles than stator poles: Concept to implementation," in IEEE Transactions on Industrial Electronics, 2010. doi: 10.1109/TIE.2009.2034678.

[16] B. Bilgin, A. Emadi, and M. Krishnamurthy, "Design considerations for switched reluctance machines with a higher number of rotor poles," IEEE

Transactions on Industrial Electronics, vol. 59, no. 10, 2012, doi: 10.1109/TIE.2011.2141102.

[17] B. Bilgin, A. Emadi, and M. Krishnamurthy, "Comprehensive evaluation of the dynamic performance of a 6/10 SRM for traction application in PHEVs," IEEE Transactions on Industrial Electronics, vol. 60, no. 7, 2013, doi: 10.1109/TIE.2012.2196015.

[18] J. Lin, N. Scho eld, and A. Emadi, "External-Rotor 6-10 Switched Reluctance Motor for an Electric Bicycle," IEEE Transactions on Transportation Electri cation, vol. 1, no. 4, 2015, doi: 10.1109/TTE.2015.2502543.

[19] J. Dang, J. R. Mayor, S. A. Semidey, R. G. Harley, T. G. Habetler, and J. A. Restrepo, "Practical considerations for the design and construction of a high-speed SRM with a  ux-bridge rotor," IEEE Trans Ind Appl, vol. 51, no. 6, 2015, doi: 10.1109/TIA.2015.2445813.

[20] K. Kiyota, T. Kakishima, A. Chiba, and M. A. Rahman, "Cylindrical rotor design for acoustic noise and windage loss reduction in switched reluctance motor for HEV applications," IEEE Trans Ind Appl, vol. 52, no. 1, 2016, doi: 10.1109/TIA.2015.2466558.

[21] X. Sun, K. Diao, G. Lei, Y. Guo, and J. Zhu, "Study on Segmented-Rotor Switched Reluctance Motors With Different Rotor Pole Numbers for BSG System of Hybrid Electric Vehicles," IEEE Trans Veh Technol, vol. 68, no. 6, pp. 5537–5547, Jun. 2019, doi: 10.1109/TVT.2019.2913279.

[22] Z. Xu, J. Liu, M. J. Kim, D. H. Lee, and J. W. Ahn, "Characteristics Analysis and Comparison of Conventional and Segmental Rotor Type 12/8 Switched Reluctance Motors," in IEEE Transactions on Industry Applications, 2019. doi: 10.1109/TIA.2018.2859324.

[23] B. C. Mecrow, E. A. El-Kharashi, J. W. Finch, and A. G. Jack, "Preliminary performance evaluation of switched reluctance motors with segmental rotors," IEEE Transactions on Energy Conversion, vol. 19, no. 4, 2004, doi: 10.1109/TEC.2004.837290.

[24] B. C. Mecrow, J. W. Finch, E. A. El-Kharashi, and A. G. Jack, "Switched reluctance motors with segmental rotors," IEE Proceedings - Electric Power Applications, vol. 149, no. 4, p. 245, 2002, doi: 10.1049/ip-epa:20020345.

[25] A. J. Hutton and T. J. E. Miller, "Use of  ux screens

in switched reluctance motors," in IEE Conference Publication, 1989.

[26] Y. G. Dessouky, B. W. Williams, and J. E. Fletcher, "Conducting screen utilisation in switched reluctance motors," IEEE Transactions on Energy Conversion, vol. 14, no. 4, pp. 946–951, 1999, doi: 10.1109/60.815012.

[27] R. Hamdy, J. E. Fletcher, B. W. Williams, and S. J. Finney, "High-speed performance improvements of a two-phase switched reluctance machine utilizing rotor-conducting screens," IEEE Transactions on Energy Conversion, vol. 17, no. 4, 2002, doi: 10.1109/TEC.2002.805202.

[28] M. M. Mahmoud, J. E. Fletcher, and B. W. Williams, "Evaluation of rotor conducting screens on the single-phase switched reluctance machine," Electric Power Components and Systems, vol. 34, no. 2, 2006, doi: 10.1080/15325000500244674.

[29] S. Xu, L. Tao, G. Han, and C. Liu, "A Novel Driven Scheme Regarding to Current Dynamics Enhancement for Switched Reluctance Motor System," IEEE Transactions on Transportation Electri cation, 2023, doi: 10.1109/TTE.2023.3243176.

[30] D. Roy and M. Sengupta, "An Experimentally Validated Novel Analytical Approach for Modeling of a Saturated Switched Reluctance Motor," IEEE Trans Magn, vol. 58, no. 12, 2022, doi: 10.1109/TMAG.2022.3210155.

[31] G. Watthewaduge and B. Bilgin, "Reluctance Mesh-Based Magnetic Equivalent Circuit Modeling of Switched Reluctance Motors for Static and Dynamic Analysis," IEEE Transactions on Transportation Electri cation, vol. 8, no. 2, 2022, doi: 10.1109/TTE.2021.3132885.

[32] N. K. Sheth and K. R. Rajagopal, "Calculation of the  ux-linkage characteristics of a switched reluctance motor by  ux tube method," IEEE Trans Magn, vol. 41, no. 10, 2005, doi: 10.1109/TMAG.2005.854865.

[33] R. Krishnan, Switched reluctance motor drives: Modeling, simulation, analysis, design, and applications. 2017. doi: 10.1201/9781420041644.

[34] P. Materu and R. Krishnan, "Analytical prediction of SRM inductance pro le and steady-state average torque," in Conference Record - IAS Annual Meeting (IEEE Industry Applications Society), 1990. doi: 10.1109/ias.1990.152189.